



Analysis and Safety Design of Aero-Engine Rotor Dynamic Response with Multiple Loads Due to Fan Blade off

Jie Fu¹, Chao Li², Jie Hong^{1,2}(✉), and Yanhong Ma²

¹ School of Energy and Power Engineering, Beihang University, Beijing 100191, People's Republic of China
sy2032102@buaa.edu.cn

² Research Institute of Aero-Engine, Beihang University, Beijing 100191, People's Republic of China

Abstract. After the blade losing, the aero-engine rotor system is subjected to multiple loads, including sudden unbalance excitation, angular acceleration excitation caused by time-varying speed, and rub-impact excitation due to the fan blade off (FBO), which results in a complex dynamic characteristic of the rotor system. At present, the dynamic response mechanism analysis and high-precision simulation results in this case are not complete, which seriously restricts the safety design and verification in the engine development process. This paper analyzes the load characteristics of the rotor when FBO occurs. Then the dynamic equation of inertia asymmetric rotor is carried out considering the combined action of multiple loads. the dynamic response analysis model of the low-pressure rotor of the turbofan engine with the condition of blade loss is established, the dynamic response of inertia symmetric rotor and inertia asymmetric rotor are compared and studied. A safety design idea of the support structure is proposed according to the characteristics of the inertia asymmetric rotor structure. This research shows that after the FBO occurs, the vibration response of the rotor increases sharply when it decelerates passing the critical speed, and the rotor system appears backward whirl frequency with the action of multiple loads. Compared with the inertia symmetric rotor, the inertia asymmetric rotor is more prone to appear backward whirl characteristics. According to the characteristics of inertia asymmetric rotor load with multiple loads, this paper changes the dynamic characteristics of rotor system by reducing the support stiffness, and increases the support damping to improve the energy dissipation, so as to reduce the vibration response of the inertia asymmetric rotor and to ensure the integrity of the support structure after blade loss.

Keywords: Rotor dynamics · Fan blade off · Inertia asymmetry · Rub-impact · Safety design

1 Introduction

Fan Blade Off (FBO) is a severe safety accident in the aero-engine. The study of FBO has always been an important part of aero-engine safety design. After FBO occurs, the diameter moments of inertia of the blade-disk structure are no longer equal in different directions due to the FBO, and show strong inertia asymmetry. In the meanwhile, the rotor system is subject to the combined action of multiple loads (sudden unbalance excitation, angular acceleration excitation caused by speed change, and rub-impact excitation) [1]. The action mechanism of various loads on the dynamic response of asymmetric rotor system and the interaction mechanism of various loads under strong nonlinear conditions make it very difficult for researchers to accurately obtain the rotor dynamic characteristics with the FBO.

For the study of rotor load excitation with FBO, the early Genta [2] took Jeffcott rotor as the research object, and studied the vibration response of the rotor with sudden impact load instead of the load excitation after FBO occurs. For the complex rotor system, Ren Xingmin [3], Gu Jialiu [4] calculated and analyzed the sudden unbalance response by using the improved transfer matrix method. With the in-depth research, it is found that the inertia asymmetry of the disk will occur after the blade is lost.

Yu [1] established the dynamic model of the inertia asymmetric disk, and found that the mass matrix and gyroscopic matrix of the inertia asymmetric disk are time-varying. Liu Di [5] established the modal characteristic analysis method of inertia asymmetric rotor through Hill infinite determinant to analyze the dynamic response characteristics of inertia asymmetric rotor considering time-varying speed. Ishida et al. [6] established a complex rotor model and analyzed the impact of inertia asymmetry characteristics on the dynamic characteristics of the rotor system when FBO events occurs.

After the blade is lost, the vibration amplitude of the rotor system will increase sharply, which will cause rub-impact between rotor and stator. Rub-impact will produce impact, friction and constraint effects on the rotor system, and make complex vibration phenomena to the rotor system [7]. Beatty [8] established a piecewise linear rub-impact force model for the first time, and studied the typical rub-impact characteristics. Zhang Siqi [9] gave a detailed description of the process of rotor–stator rub-impact, and found that the rotor–stator rub-impact presented nonlinear characteristics through numerical simulation. Liu Di [10] studied the rub-impact characteristics of rotor under sudden unbalance excitation from the perspective of complex nonlinearity, indicating that severe rub-impact will lead to backward whirl.

The excessive reaction forces of the support after FBO will seriously threaten the structural integrity of the rotor system [11]. Li Chao [12] designed a buffer damping support structure to reduce the reaction forces of the support of the rotor system with FBO; Hong Jie [13] proposed a safety design strategy, which can effectively reduce the vibration of the fan disk by changing the bearing position and the support stiffness.

The above research on the dynamic characteristics of rotor system when FBO occurs is mostly focused on the impact of sudden unbalance load generated by FBO events on the rotor system, while the specific research on the load characteristics of rotor system after blade loss is less. In addition, there is little research on the inertial asymmetry of the rotor with the combined action of multiple loads (sudden unbalance excitation, angular acceleration excitation caused by time-varying speed and rub-impact excitation) after

FBO occurs, which results that there is no clear concept about the dynamic response of the inertia asymmetry rotor with the excitation of multiple loads after FBO occurs. In this paper, when FBO occurs, the load characteristics of the rotor system are described with the low-pressure rotor structure of a high bypass ratio turbofan engine. The dynamic model of the inertial asymmetric rotor system is established considering the action of multiple loads, the dynamic response of the inertial symmetric rotor and the inertial asymmetric rotor with the action of multiple load excitation are compared and analyzed. The safety design strategy of inertia asymmetric rotor is proposed, which provides certain theoretical and technical support for the safety research of aeroengine.

2 Description of Rotor Load Characteristics After FBO

After FBO occurs, the motion process of the engine rotor system is variable and the load situation is complex. Take the high bypass ratio turbofan engine as an example. After the large diameter fan blade losing, the rotor motion state and load characteristics of aero-engine can be divided into three stages:

- 1) Before FBO occurs, the rotor system with fine assembly and balance can be considered that the center of mass (G point) coincides with the center of rotation (O point). During stable state, the rotational inertia excitation load is at a low level.
- 2) At the moment of FBO, the rotor system is impacted by sudden unbalance. Due to the lack of blade, the diameter moment of inertia of the blade-disk structure shows asymmetry, resulting in the inertia asymmetry ($J_x \neq J_y$).
- 3) After the blade is lost, the speed of the rotor system will change in a short time, and the rotor system will be affected by the angular acceleration caused by the time-varying speed; The center of mass (G point) will no longer coincide with the center of rotation (O point), which will cause the center of mass deviation, and the rotor system will also subject to large unbalanced rotation excitation. The rotor unbalance vibration makes the rotor amplitude exceed the blade-casing clearance. The blade will contact

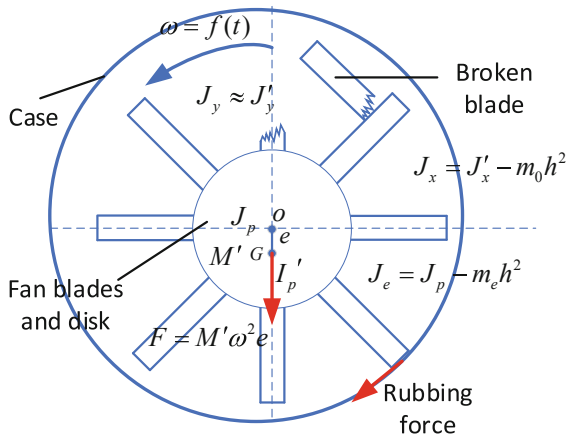


Fig. 1. Variation of rotor load characteristics after FBO.

and rub the casing. Therefore, the fan casing will generate additional rubbing force on the rotor system, as shown in Fig. 1.

3 Action Mechanism of Multiple Loads with FBO

3.1 Sudden Unbalance Load

Before FBO occurs, the initial unbalance of the rotor system is small (about $100g \cdot mm$), and the rotation excitation is small. After the blade is lost, the unbalance increases significantly (the unbalance can reach $10^6g \cdot mm$), and the center of mass will suddenly deviate at the moment of FBO, which results in a sudden unbalance load.

After FBO occurs, the rotation speed will rapidly reduce to the windmill speed. With the rapid reduction of speed, the rotor system will be affected by the tangential load ($F_T = m_e e \ddot{\theta}$) caused by the time-varying speed (Fig. 2).

The expression is given in Eq. (1):

$$P(t) = \begin{cases} \{0, 0\}^T & t < t_{B-off} \\ m_e e \{ \ddot{\theta} \sin \theta + \dot{\theta}^2 \cos \theta, -\ddot{\theta} \cos \theta + \dot{\theta}^2 \sin \theta \} & t \geq t_{B-off} \end{cases} \quad (1)$$

wherein, m_e represents the mass of the fan disk after FBO, e represents the eccentricity, θ represents the phase angle of the fan disk, and t_{B-off} represents the moment of FBO.

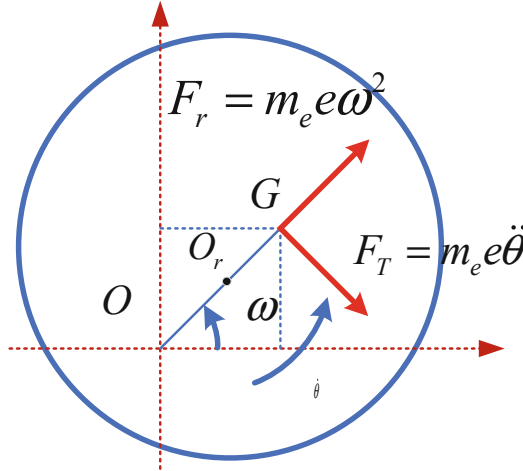


Fig. 2. The load of unbalanced rotor during time-varying speed.

3.2 Inertial Asymmetric Disk

FBO makes the blade disk structure mass eccentricity e . The method proposed in reference [1] to analyze the inertial asymmetric disk. According to the theorem of parallel

axis, the polar moment of inertia around O_r point is $J_e = J_p - mh^2$, the diameter moment of inertia around inertia main shaft are $J_x = J_p/2 - mh^2$, $J_y = J_p/2$. the diameter moment of inertia in both directions are not equal, which are called inertia asymmetric, as shown in Fig. 3.

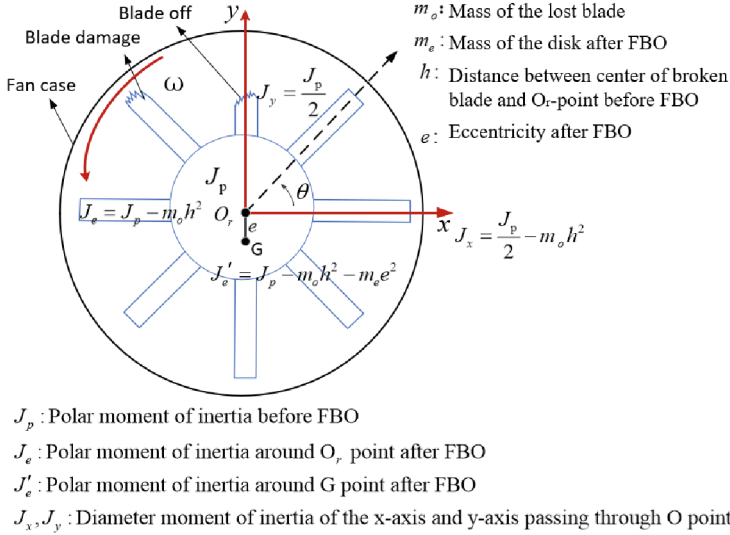


Fig. 3. The inertial asymmetric characteristics of the fan disk.

The control equation of the rotor system in the absolute coordinate system is established with the *Lagrange* energy method, as shown in Eq. (2):

$$\frac{d}{dt} \left(\frac{\partial T}{\partial \dot{q}} \right) - \frac{\partial T}{\partial q} + \frac{\partial U}{\partial q} = Q \quad (2)$$

$q = [x, y, \theta_x, \theta_y]^T$ is the radial and angular freedom of the disk.

The kinetic energy expression of the asymmetric disk is shown in Eq. (3):

$$T_d = \frac{1}{2} m (\dot{x}^2 + \dot{y}^2) + \frac{1}{2} J_x (\dot{\theta}_x \cos \omega t + \dot{\theta}_y \sin \omega t)^2 + \frac{1}{2} J_y (\dot{\theta}_x \sin \omega t - \dot{\theta}_y \cos \omega t)^2 + \frac{1}{2} (J_x + J_y) [\omega^2 + \omega (\dot{\theta}_x \theta_y - \dot{\theta}_y \theta_x)] \quad (3)$$

Equation (4) defines the average diameter moment of inertia J and Eq. (5) defines the inertia unsymmetrical ΔJ .

$$J = (J_x + J_y)/2 \quad (4)$$

$$\Delta J = (J_y - J_x)/2 \quad (5)$$

Substitute Eq. (4) and Eq. (5) to obtain the fan disk kinematics equation, as shown in Eq. (6):

$$(M_{disc} + M_{disc-c} \cos 2\omega t + M_{disc-s} \sin 2\omega t)\ddot{q} + (G_{disc} + G_{disc-c} \cos 2\omega t + G_{disc-s} \sin 2\omega t)\dot{q} = 0 \quad (6)$$

wherein, M_{disc} and G_{disc} are the mass matrix and gyro matrix respectively, $M_{disc-c} \cos 2\omega t$ and $M_{disc-s} \sin 2\omega t$ are the time-varying mass matrix of fan disk, $G_{disc-c} \cos 2\omega t$, $G_{disc-s} \sin 2\omega t$ are the time-varying gyro matrix of the disk.

$$M_{disc} = \begin{bmatrix} m & & & \\ & m & & \\ & & J & \\ & & & J \end{bmatrix}, G_{disc} = \begin{bmatrix} 0 & & & \\ & 0 & & \\ & & 0 & 2J\omega \\ & & -2J\omega & 0 \end{bmatrix}.$$

$$M_{disc-c} = \Delta J \begin{bmatrix} 0 & & & \\ & 0 & & \\ & & -1 & \\ & & & 1 \end{bmatrix}, G_{disc-c} = 2\omega\Delta J \begin{bmatrix} 0 & & & \\ & 0 & & \\ & & 0 & -1 \\ & & -1 & 0 \end{bmatrix}.$$

$$M_{disc-s} = \Delta J \begin{bmatrix} 0 & & & \\ & 0 & & \\ & & 0 & -1 \\ & & -1 & 0 \end{bmatrix}, G_{disc-s} = 2\omega\Delta J \begin{bmatrix} 0 & & & \\ & 0 & & \\ & & 1 & \\ & & & -1 \end{bmatrix}.$$

3.3 Rub-Impact Excitation

After the blade is lost, the fan casing and the blade collide with each other, resulting in mutual force. In this paper, the method proposed in reference [14] will be used to obtain the rubbing force between the blade and the casing. The origin (i.e. the rotating center of the disk) is O , the geometric center is O_r , the distance from the blade tip to the geometric center O_r is r , and the displacement of geometric center O_r in the x and y directions is recorded as x_1 and y_1 , respectively. Take the i -th blade for analysis. At the moment of t , the phase angle φ_i of the i -th blade is calculated as shown in Eq. (7):

$$\varphi_i = \omega t + 2\pi(i-1)/n \quad (7)$$

n is the number of blades and ω is the rotor speed.

Equation (8) defines the distance from the i -th blade tip to the center of rotation (O point):

$$r'_i = \sqrt{(x_1 + r \cos \varphi_i)^2 + (y_1 + r \sin \varphi_i)^2} \quad (8)$$

ϕ_i is the included angle between r'_i with the x direction.

As shown in Fig. 4, the velocities of the disk geometric center in the x and y directions are respectively defined as v_{x1} and v_{y1} . Therefore, the velocities of the i -th blade tip in the x and y directions are shown in Eq. (9):

$$\begin{cases} v_{xi} = -v_{x1} + \omega r \sin \varphi_i \\ v_{yi} = -v_{y1} + \omega r \cos \varphi_i \end{cases} \quad (9)$$

The speed of the i -th blade tip relative to the casing is calculated as follows in Eq. (10):

$$v_{\tau i} = v_{yi} \cos \Phi_i + v_{xi} \sin \Phi_i \quad (10)$$

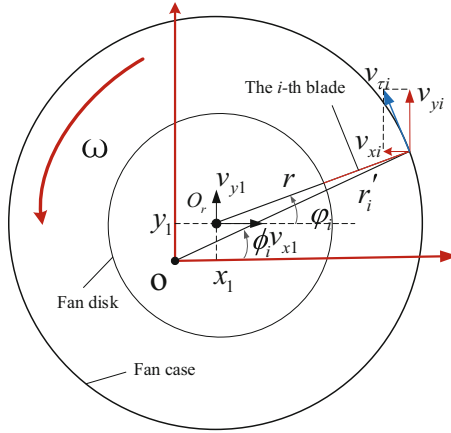


Fig. 4. Speed of the blade tip relative to fan case.

The rubbing force between fan blade and casing is decomposed into rubbing normal force and rubbing tangential force, as shown in Fig. 5. The rubbing normal force adopts linear elastic model, and the rubbing tangential force adopts Coulomb friction model. Establish rubbing criteria: $P_i = r'_i - r - r_0$. If $P_i \leq 0$, it means that the fan blade is not in contact with the fan casing, and there is no rotor-stator rubbing; If $P_i > 0$, it means that there is no clearance between the fan blade and the casing, and there has been friction. If rub-impact occurs, the fan casing will generate radial rubbing force $F_{ni} = k_c P_i$ and tangential rubbing force $F_{\tau i} = \mu F_{ni}$ on the rotor system, which are decomposed in the x and y directions shown in Eq. (11):

$$\begin{cases} F_{xi} = k_c f_{xi} \\ F_{yi} = k_c f_{yi} \end{cases}, \begin{cases} f_{xi} = -H(P_i)(P_i \cos \Phi_i - \text{sign}(v_{\tau i})\mu P_i \cos \Phi_i) \\ f_{yi} = -H(P_i)(P_i \sin \Phi_i + \text{sign}(v_{\tau i})\mu P_i \sin \Phi_i) \end{cases} \quad (11)$$

$$\text{In Eq. (11): } H(P_i) = \begin{cases} 1 & P > 0 \\ 0 & P \leq 0 \end{cases}, \text{sign}(v_{\tau i}) = \begin{cases} 1 & v_{\tau i} > 0 \\ 0 & v_{\tau i} = 0 \\ -1 & v_{\tau i} < 0 \end{cases}.$$

Translate the component force in the x and y directions to the geometric center O_r of the disk, and obtain the friction force (shown in Eq. (12)) of the rotor blade disk in

the x and y directions. In this paper, it did not consider the torque acting on the center of disk:

$$\begin{cases} F_x = k_c f_x \\ F_y = k_c f_y \end{cases}, \quad f_x = \sum_{i=0}^n f_{xi}, \quad f_y = \sum_{i=0}^n f_{yi} \quad (12)$$

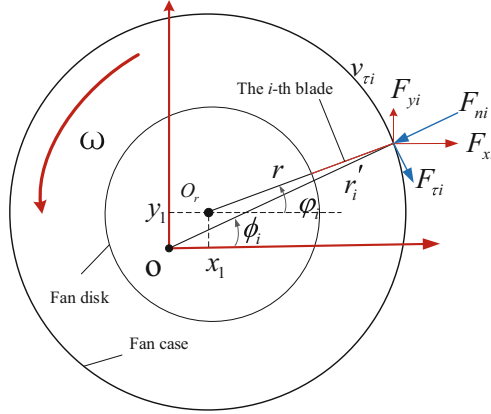


Fig. 5. Rubbing force between the blade and fan case.

3.4 Rotor Dynamics Model with Multiple Loads

After FBO occurs, the inertia symmetric rotor system becomes an inertia asymmetric one. The rotor system is subject to the combined action of multiple loads (sudden impact load, large unbalance rotating excitation, angular acceleration excitation and rub-impact excitation). Write multiple load excitation in the form of Eq. (11):

$$P(t) = \begin{cases} m_0 e \left\{ \dot{\theta}^2 \cos \theta, \dot{\theta}^2 \sin \theta \right\}^T & t < t_{B-off} \\ \left\{ m_e e \dot{\theta}^2 \cos \theta + p_x, m_e e \dot{\theta}^2 \sin \theta + p_y \right\}^T & t_{B-off} \leq t < t_1 \\ \left\{ m_e e \ddot{\theta} \sin \theta + m_e e \dot{\theta}^2 \cos \theta + p_x, -m_e e \ddot{\theta} \cos \theta + m_e e \dot{\theta}^2 \sin \theta + p_y \right\}^T & t_1 \leq t < t_2 \\ \left\{ m_e e \dot{\theta}^2 \cos \theta + p_x, m_e e \dot{\theta}^2 \sin \theta + p_y \right\}^T & t_2 \leq t \leq t_{end} \end{cases} \quad (13)$$

wherein, m_o is the mass of the fan disk before the blade losing, m_e is the mass of the fan disk after FBO, e is the eccentricity, θ is the phase angle of the fan disk, p_x, p_y are the component of the friction force in the x and y directions, t_{B-off} is the moment of FBO, t_1 is the time when the speed starts to decrease, t_2 is the time when the speed reaches the speed of the windmill, and t_{end} is the end time.

Therefore, the rotor dynamics equation of inertia symmetric rotor with multiple loads is shown in Eq. (14):

$$M\ddot{q} + (C + G)\dot{q} + Kq = P(t) \quad (14)$$

And the rotor dynamics equation of inertia asymmetric rotor with multiple loads after FBO is given in Eq. (15):

$$\begin{aligned} & (M_{disc} + M_{disc-c} \cos 2\omega t + M_{disc-s} \sin 2\omega t)\ddot{q} \\ & + (C + G_{disc} + G_{disc-c} \cos 2\omega t + G_{disc-s} \sin 2\omega t)\dot{q} + Kq = P(t) \end{aligned} \quad (15)$$

$P(t)$ refers to multiple load excitation of rotor system, including initial unbalance excitation, sudden unbalance excitation, angular acceleration excitation, large unbalance excitation and rub-impact excitation.

4 Modeling and Analysis Method of Low-Pressure Rotor

4.1 Establishment of Low-Pressure Rotor Model

Referring to the low-pressure rotor of a typical high bypass ratio turbofan engine, a finite element model is established. The low-pressure rotor is mainly composed of 30 fan blades, 4-stage compressor, 5-stage low-pressure turbine, fan disk and compressor structure, fan stub shaft, low-pressure turbine shaft, turbine disk and 3 fulcrums, as shown in Fig. 6.

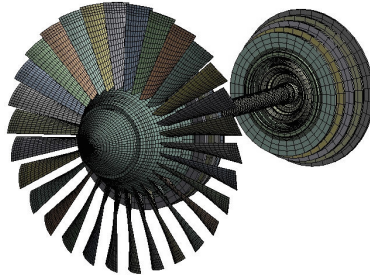


Fig. 6. LP rotor finite element model.

The modal characteristics of the rotor system are analyzed. The first order critical speed of the rotor system is $\omega_1 = 4900 \text{ rpm}$ and the mode shape is the pitch vibration of fan; The second order critical speed is $\omega_2 = 5964 \text{ rpm}$, and the mode shape is the translation motion of the turbine; The third order critical speed is $\omega_3 = 18028 \text{ rpm}$, and the mode shape is the overall bending vibration. As shown in Fig. 7, the working speed of the rotor system is 9000 rpm . The critical speed of the overall bending vibration mode is designed above the working speed. The rotor system does not go through the overall bending critical speed during the acceleration and deceleration process, which is in accordance with the engineering design.

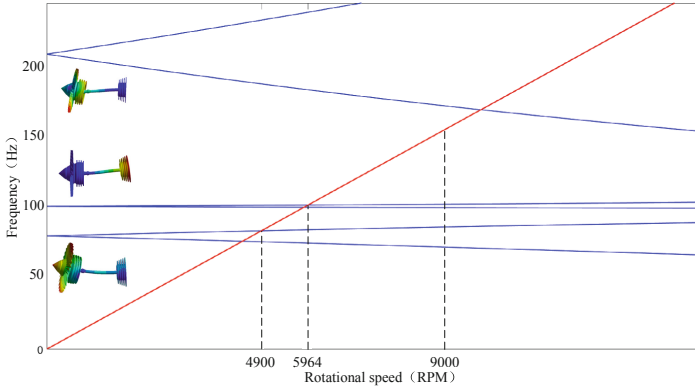


Fig. 7. The LP rotor resonance speed distribution.

4.2 Dynamic Response Analysis Method

First, the three-dimensional solid model of LP rotor is established through finite element analysis software, and the established model is output to the [K], [C], [M], [G] matrix in HBMAT format.

Use the simulation software to convert the matrix of HBMAT format into the rotor dynamics matrix. The dynamic equations of inertia symmetric rotor and inertia asymmetric rotor are constructed in the simulation software based on Sect. 3.4, and the mechanical boundary conditions of multiple loads are applied to the rotor system.

Finally, the established rotor dynamics equation is solved by the Newmark- β method. The dynamic analysis method is shown in Fig. 8.

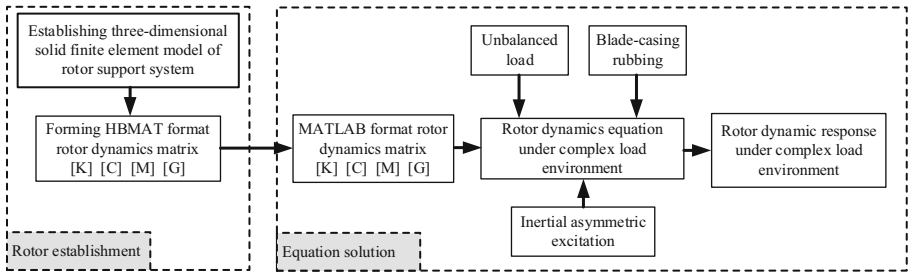


Fig. 8. Dynamic analysis method.

5 Analysis of Rotor Dynamic Response with Multiple Load Excitation

The radius of the fan is 460 mm, and the rub-impact clearance is 2.5 mm (if the radial vibration displacement of the fan blade is greater than 2.5 mm, the rotor rub-impact occurs). The rigidity of the fan casing is $K=2 \times 10^7 N/m$, and the friction coefficient is $\mu = 0.2$.

In the initial state, the rotor runs stably at the working speed. When FBO occurs, the rotor system speed will rapidly reduce to the windmill speed in a short time, and keep the windmill speed rotating continuously. The rotation speed-time diagram is shown in Fig. 9.

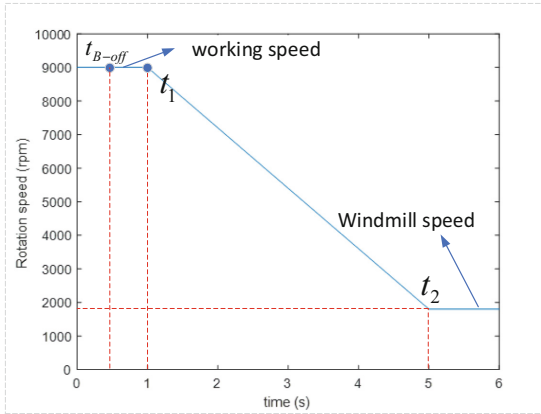


Fig. 9. Rotation speed-time diagram.

5.1 Inertia Symmetric Rotor

From the Sect. 3.4, we can get the dynamic equation of inertia symmetric rotor, as shown in Eq. (14).

In this paper, Newmark- β method is adopted to solve Eq. (14), and the dynamic response law of the inertia symmetric rotor with multiple loads is obtained.

Time-Frequency Displacement Response. Figure 10(a) and Fig. 10(b) show the horizontal and vertical displacement response of the fan disk in time domain. It can be seen that the initial unbalance of the fan disk is small before the blade lost, and the vibration amplitude is small for the action of the initial unbalance load. After FBO occurs, the amplitude of the fan disk increases sharply. When passing the first critical speed, the amplitude of the fan disk reaches a peak. Figure 10(c) shows the amplitude of the fan disk in time domain. From the Fig. 10(c), we can see that the peak amplitude of the fan disk in time domain reaches 2.73 mm, which exceeds the clearance between the fan blade and the fan casing (2.5 mm).

Rub-impact is a continuous process. Figure 10(d) is the vibration response of the fan disk in frequency domain. In Fig. 10(d), it can be seen that the main frequency 81.33 Hz is the frequency when the rotor system passes the first critical speed. A lot of clutter in the frequency 85 Hz–100 Hz are caused by the rub-impact. In the frequency domain figure (Fig. 10(d)), it can be seen that the first-order backward whirl frequency of the rotor system is 75.17 Hz, which is due to the backward whirl frequency caused by the action of the tangential rubbing force when rub-impact occurs.

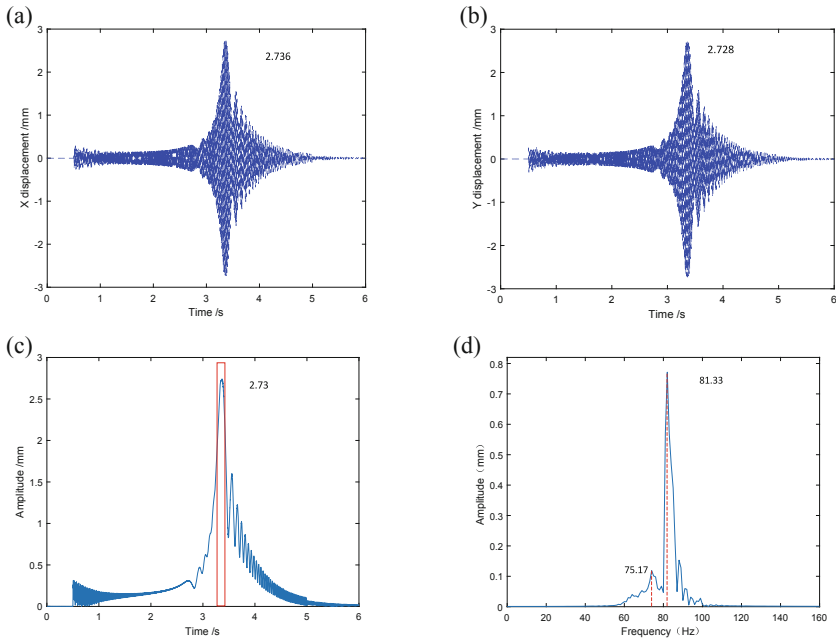


Fig. 10. The vibration response of the inertia symmetric fan disk (a) horizontal displacement in time domain (b) vertical displacement in time domain (c) vibration amplitude in time domain (d) response in frequency domain.

The Reaction Forces of the Supports. Figure 11 shows the reaction forces of No.1, No.2 and No.3 supports of inertia symmetric rotor in time domain with the action of multiple loads. In the normal working conditions, the amplitude of the supports' reaction forces is small due to the effect of initial unbalanced load. When FBO occurs, the supports' reaction forces increase sharply. When passing the first critical speed, the reaction forces of supports reach the peak value, the reaction force of No.1 support reaches $9.65 \times 10^4 N$, the reaction force of No.2 support reaches $5.944 \times 10^4 N$, and the maximum the reaction force of No.3 support reaches $6.401 \times 10^4 N$;

The second mode shape of the rotor system is the translation motion of the turbine, which is small effect on the fan (including No.1 support and No.2 support). On the contrary, it has a large impact on the turbine rear support (No.3 support). When passing the second critical speed, the reaction force of No.3 support reaches a peak value of about $4.068 \times 10^4 N$.

To sum up, when the rotor system passes the critical speed, the supports' reaction forces of the rotor system reaches the peak value. Therefore, when the rotor decelerates beyond the critical speed point, the vibration response of the rotor is the largest and it is the most dangerous point, which needs to be focused on.

Rub-Impact Characteristics. The rub-impact characteristics of the rotor system are analyzed, and axis orbit of inertia symmetric rotor during rubbing in Fig. 12 is obtained.

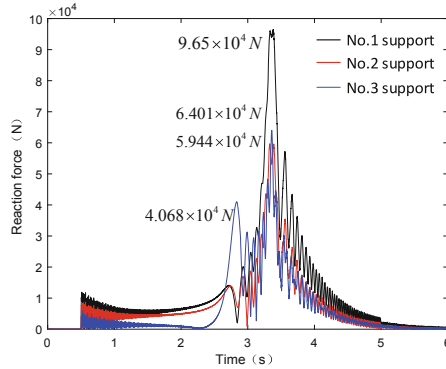


Fig. 11. The reaction forces of the supports of the inertia symmetric rotor in time domain.

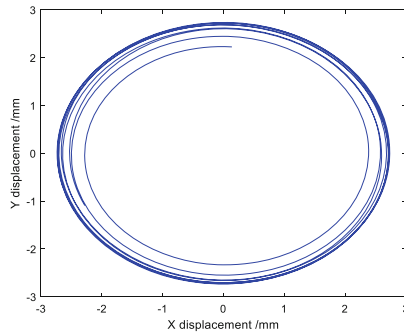


Fig. 12. Axis orbit of inertia symmetric rotor during rubbing.

Figure 12 shows axis orbit of the fan disk of the inertia symmetric rotor system during rubbing. From the Fig. 12, it can be seen that the form of rubbing between the fan blade and the casing is full annular rub, and the rubbing is continuously.

5.2 Inertia Asymmetric Rotor

The mutually orthogonal diameter moments of inertia are no longer equal due to the fan losing. At the rotating state, the mass matrix and gyro matrix of the rotor system are time-varying instead of constant.

From the Sect. 3.4, we can get the dynamic equation of inertia asymmetric rotor, as shown in Eq. (15).

In this paper, Newmark- β method is adopted to solve Eq. (14), and the dynamic response law of the inertia asymmetric rotor with multiple loads is obtained.

Time–frequency displacement response. Figure 13(a) and Fig. 13(b) show the horizontal and vertical displacement response of the fan disk in time domain. It can be seen that the response of inertia asymmetric rotor with multiple load excitation is similar to that of inertia symmetric rotor. the initial unbalance of the fan disk is small before the

blade lost, and the vibration amplitude is small for the action of the initial unbalance load. After FBO occurs, the amplitude of the fan disk increases sharply. When passing the first critical speed, the maximum horizontal displacement reaches 2.921 mm, the maximum vertical displacement reaches 3.692 mm. Figure 13(c) shows the amplitude of the fan disk in time domain. From the Fig. 13(c), we can see that the peak amplitude of the fan disk in time domain reaches 3.797 mm, which exceeds the rotor-static clearance of 2.5 mm, and the rotor-static friction occurs between the fan blade and the casing.

Figure 13(d) is the vibration response of the fan disk in frequency domain. In Fig. 13(d), it can be seen that the main frequency 82 Hz is the frequency when the rotor system passes the first critical speed. From the Fig. 10(d), it also can be seen that the first-order backward whirl frequency of the rotor system is 76 Hz, which is caused by the action of the tangential rubbing force when rub-impact occurs.

Compared with inertia symmetric rotor, inertia asymmetric rotor is subject to more serious rub-impact and represents more obvious rub-impact characteristics. It can be seen from the Fig. 13(d) that there are two main frequencies in the rotor system with the excitation of multiple loads: 82 Hz and 76 Hz. They are the first critical speed (forward whirl) frequency and the first backward whirl frequency, which indicate that the inertia asymmetric rotor has serious rub-impact between rotor and stator with the excitation of multiple loads, directly resulting in the backward whirl in the rotor system.

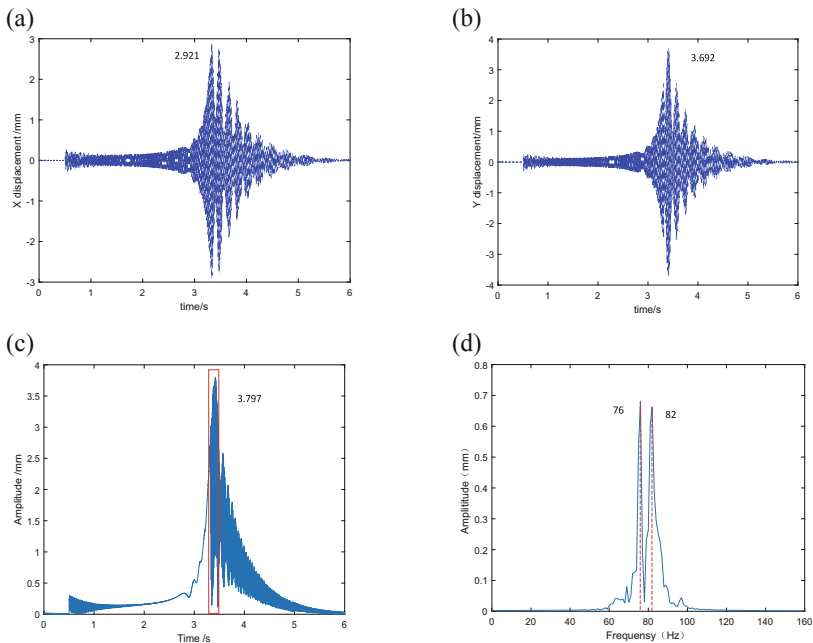


Fig. 13. The vibration response of the inertia asymmetric fan disk (a) horizontal displacement in time domain (b) vertical displacement in time domain (c) vibration amplitude in time domain (d) response in frequency domain.

The Reaction Forces of the Supports. Figure 14 shows the reaction forces of No.1, No.2 and No.3 supports of inertia asymmetric rotor in time domain with the action of multiple loads. From the Fig. 14, the supports' reaction forces of inertia asymmetric rotor are similar to the supports' reaction forces of the inertia symmetric rotor. In the normal working conditions, the amplitude of the supports' reaction forces is small due to the effect of initial unbalanced load. When FBO occurs, the supports' reaction forces increase sharply. When passing the first critical speed, the reaction forces of supports reach the peak value, the reaction force of No.1 support reaches $1.349 \times 10^5 N$, the reaction force of No.2 support reaches $8.245 \times 10^4 N$, and the maximum the reaction force of No.3 support reaches $8.194 \times 10^4 N$;

The second mode shape of the rotor system is the translation motion of the turbine, which is small effect on the fan (including No.1 support and No.2 support). On the contrary, it has a large impact on the turbine rear support (No.3 support). When passing the second critical speed, the reaction force of No.3 support reaches a peak value of about $4.196 \times 10^4 N$.

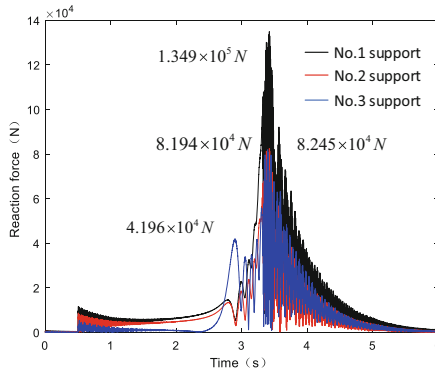


Fig. 14. The reaction forces of the supports of the inertia asymmetric rotor in time domain.

Table 1 is obtained by comparing the peak of the supports' reaction forces of the inertia asymmetric rotor system with the peak of the supports' reaction forces of the inertia symmetric rotor system with multiple load excitation.

From Table 1, compared with the peak value of the supports' reaction forces of the inertia asymmetric rotor and the peak value of the inertia symmetric rotor, the peak value of the supports' reaction forces increases. The supports' reaction forces increase more obviously at the first critical speed. Therefore, at the first critical speed, the reaction force of No.1 support increased by 39.79%, about 38400N; The reaction force of No.3 support increased by 37.85%, about 22500N; The reaction force of No.2 support increased by 28.81%, about 18440N. It has little influence on the peak of supports' reaction forces at the second critical speed.

Table 1. Peak value comparison of the supports' reaction forces with multiple loads

Support number	No.1 support	No.2 support	No.3 support (the 1st order)	No.3 support (the 2nd order)
The inertia symmetric rotor system	96500N	64010N	59440N	40680N
The inertia asymmetric rotor system	134900N	82450N	81940N	41960N
Variation	+38400N	+18440N	+22500N	+1280N
Change rate	+39.79%	+28.81%	+37.85%	+3.15%

To sum up, the inertia asymmetry will seriously affect the reaction forces of the supports, make the rotor supports bear greater reaction forces, and seriously threaten the safety of the bearing support structure.

Rub-Impact Characteristics

The rub-impact characteristics of the rotor are analyzed, mainly the axis orbit at the rub-impact stage, as shown in Fig. 15(a). Figure 15(b) shows the backward whirl characteristics of the inertia asymmetric.

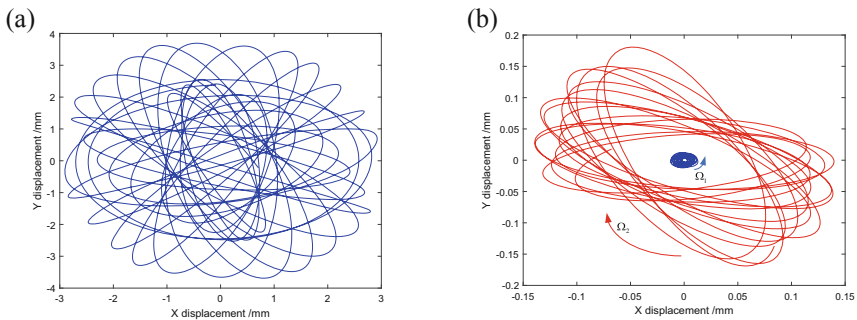


Fig. 15. Axis orbit of inertia asymmetric rotor (a) rub-impact stage, (b) backward whirl characteristics.

It can be seen from the Fig. 15(a) that the form of rubbing between the fan rotor blades and the casing is local rub. There are multiple contact-collisions and rebound-separation between blades and casing. From the Fig. 15(b), the inertia asymmetric rotor shows the backward whirl feature after the rub-impact. The whirl direction of the rotor system at the initial time is anticlockwise (forward whirl). After rub-impact, the whirl direction of the rotor system turns clockwise (backward whirl) with the action of rub-impact excitation, which is opposite to the initial whirl direction. The rotor system has the backward whirl characteristics.

Compared with the inertia symmetric rotor, the inertia asymmetric rotor has more serious rub-impact. From the Figs. 12 and 15(a), the inertia symmetric rotor mainly rubs in the form of contact non-separation full-cycle rubs, while the inertia asymmetric rotor mainly rubs in the form of contact separation local rub with multiple load excitation.

From the previous analysis, it can be seen that inertia symmetric rotor has only one backward whirl frequency with multiple load excitation, and there is no backward whirl characteristics; However, with the combined action of multiple loads, the degree of rub-impact of the inertial asymmetric rotor system is more serious, and the time of rub-impact is longer. The serious rub-impact directly leads to the backward whirl characteristics of the rotor system. Therefore, the inertial asymmetric rotor system is more prone to backward whirl than the inertial rotor system.

6 Safety Design of Support Structure

6.1 Safety Design Strategy

With the action of multiple loads, the transient response peak of the inertia asymmetric rotor system can reach above $1.3 \times 10^5 N$, which can affect the completeness of the supporting structure, and in severe cases, it can cause secondary accidents such as bearing jamming, damage to mount, shaft breakage, etc. Therefore, it is necessary to design a safety structure of the aeroengine rotor to reduce the reaction forces of supports.

- (1) The low-pressure rotor is a flexible rotor with multiple fulcrums. After FBO occurs, the No.1 support of the rotor system is the closest to the fan and its load is the largest. Therefore, the load environment of the No.1 support of the rotor system is the most severe. It is necessary to carry out safety design for it.
- (2) For modern aero-engines, the No.1 support is a roller bearing, which mainly bears radial load. Figure 16(a) and (b) shows the safety design of typical support structures at home and abroad. As can be seen from Fig. 16(a) and (b), in order to avoid secondary failure caused by excessive reaction force of support, the safety design of the fuse structure (design of thinned conical shell (e.g. Fig. 17(a)) and design of fuse bolt (e.g. Fig. 17(b))) has been carried out at the No.1 support structure, so that the rotor system can be changed from 3 to 2 fulcrums to realize the variable stiffness design of the rotor. This will change the dynamic characteristics of the rotor system, reduce the critical speed, thereby reducing the reaction force of support when the rotor passes the critical speed.
- (3) From the perspective of energy, damping will absorb the energy of rotor vibration and reduce the reaction force of support. In order to reduce the peak of support's reaction force of the inertia asymmetric rotor with the excitation of multiple loads and protect the safety of the support structure, the damping of the rotor can be appropriately increased to reduce the reaction force of support of the rotor system.

Therefore, a support structure of roller bearing is designed based on the safety design characteristics of inertia asymmetric rotor, as shown in Fig. 17(a) and (b).

The support structure mainly consists of two key structures, the fuse structure and the low stiffness structure. When the aero-engine rotor works normally, the vibration response of the rotor system is at a relatively low level. The reaction force of support

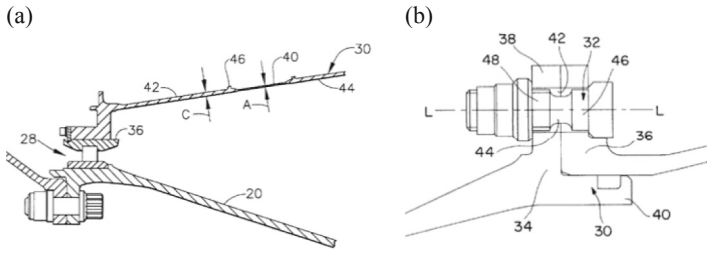


Fig. 16. Typical safety design of No.1 support structure (a) design of thinned conical shell (b) design of fuse bolt.

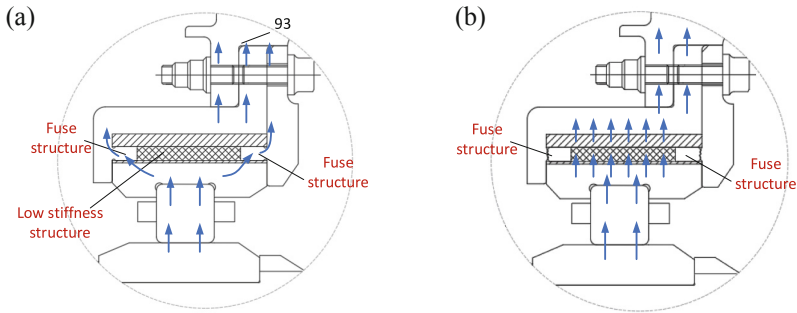


Fig. 17. A new safety design of support structure (a) working state. (b) after blade loss.

is transmitted to the left and right convex shoulder through the fulcrum bearing and the bearing outer ring (e.g. Fig. 17(a)). However, when FBO occurs, the reaction force of support is large, and the left and right convex shoulder are broken. The reaction force of support is transmitted to the elastic ring through the fulcrum bearing (e.g. Fig. 17(b)); The elastic ring is made of metal rubber with low stiffness. The metal rubber produces great damping effect and consumes vibration energy under the reaction force of support, reduces the external transmission of vibration load, and protects the support frame and mounting joint of the engine.

6.2 Effect of Reducing Support Stiffness

Change the stiffness of the No. 1 support to obtain the critical speed of the rotor system under different support stiffness. As shown in Fig. 18, which shows the change of the critical speed of the rotor system with reducing the No. 1 support stiffness.

The data in Fig. 18 is sorted out to draw Table 2.

It can be seen from Fig. 18 and Table 2 that changing the stiffness of No. 1 support has little impact on the second critical speed of the rotor system (the translation motion of the turbine mode). However, it has a great impact on the first critical speed of the rotor system (the pitch vibration of fan mode). The No. 1 support relative stiffness is reduced by 50%, and the first critical speed is reduced by 15%. When No. 1 support stiffness becomes 1% initial support stiffness, the first critical speed of the rotor is significantly

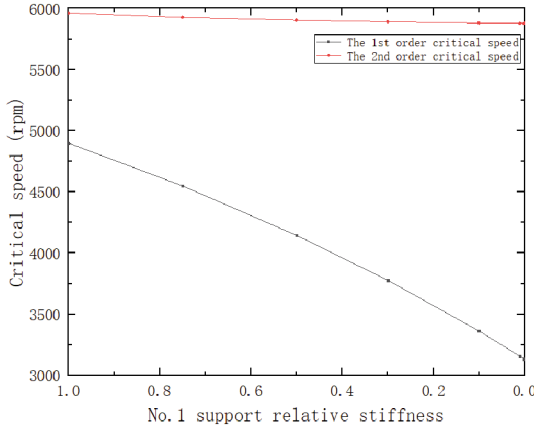


Fig. 18. Change of critical speed with reducing No. 1 support relative stiffness.

Table 2 Change of critical speed with No. 1 support relative stiffness

No. 1 support relative stiffness	1	0.75	0.5	0.3	0.1	0.01	0
First critical speed	4900	4549	4145	3778	3363	3156	3132
Percentage (%)	100	92.84	84.59	77.10	68.63	64.41	63.92
Second critical speed	5964	5928	5905	5892	5882	5879	5878
Percentage (%)	100	99.40	99.01	98.79	98.93	98.57	98.56

reduced by about 35.5%. When No. 1 support stiffness becomes 0, the support structure loses its restraint capacity, and the first critical speed decreases by 36%, which is almost the same as that of 1%.

Therefore, when the No. 1 support stiffness is two magnitudes smaller than the initial support stiffness, the No. 1 support has basically lost its restraint capacity. By reducing the No. 1 support stiffness, the critical speed of the rotor can be reduced, which will change the dynamic characteristics of the rotor and reduce the supports’ reaction forces of the rotor system.

6.3 Effect of Increasing Support Damping

According to the previous design idea (e.g. Fig. 17), after FBO occurs, increasing the support damping can increase the energy consumption of damping, reduce the peak value of the reaction force of the support, and reduce the vibration response of the rotor system.

The reaction force of No. 1 support under different damping is obtained by changing the No. 1 support damping, as shown in Fig. 19.

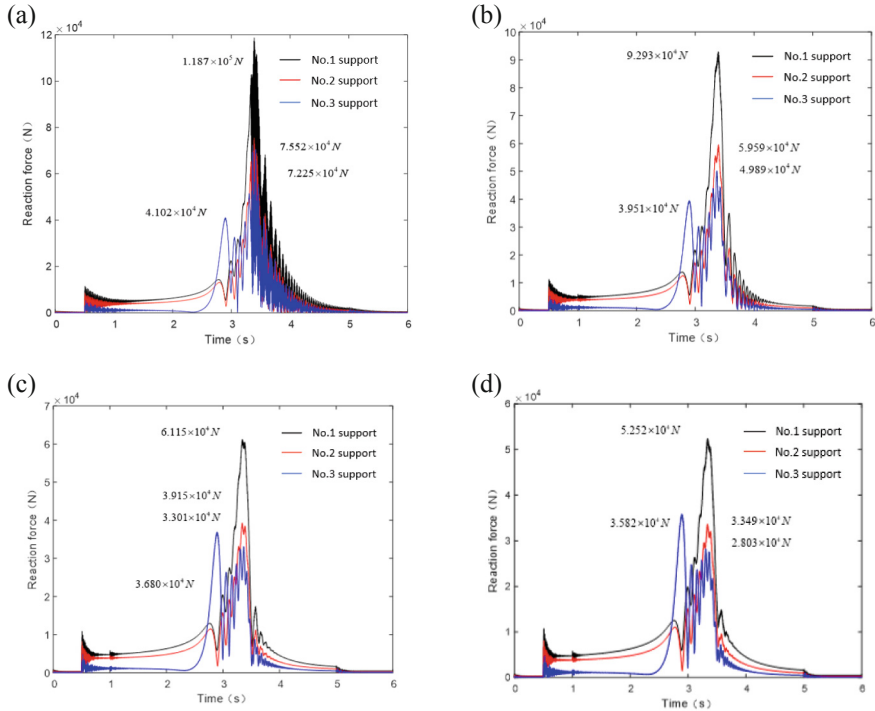


Fig. 19. The reaction forces of supports under different No.1 support damping (a) $2 \times$ support damping (b) $4 \times$ support damping (c) $8 \times$ support damping (d) $10 \times$ support damping.

The peak value of reaction forces of supports under different No.1 support damping is arranged and drawn into Table 3.

It can be seen from Fig. 19 and Table 3 that the change of No. 1 support damping can greatly change the reaction forces of rotor supports. When the No.1 support damping becomes twice the initial support damping, the peak value of No.1 support's reaction force of the rotor system decreases by 16200N, about 12%. When the No.1 support damping is increased to 10 times the initial support damping, the peak value of No.1 support's reaction force of the rotor system decreases by 82480N, 61.14%.

Through the above analysis, the dynamic characteristics of the rotor can be changed through reducing support stiffness, so as to restrain the vibration response of the rotor; The peak value of supports' reaction force of the inertia asymmetric rotor with multiple loads can be reduced by increasing the support damping, so as to reduce the vibration response of the rotor and ensure the structural integrity of the engine.

Table 3 The peak value of each support's reaction force under different No.1 support damping

Support number	No.1 support	No.2 support	No.3 support (the 1st order)	No.3 support (the 2nd order)
Initial No.1 support damping	134900N	82450N	81940N	41960N
2 × support damping	118700N	75520N	72250N	41020N
Change rate (%)	-12.01	-8.41	-11.83	-2.24
4 × support damping	92930N	59590N	49890N	39510N
Change rate (%)	-31.11	-27.73	-39.11	-5.84
8 × support damping	61150N	39150N	33010N	36800N
Change rate (%)	-54.67	-52.52	-59.71	-12.30
10 × support damping	52420N	33490N	28030N	35820N
Change rate (%)	-61.14	-59.38	-65.79	-14.63

7 Conclusion

In this paper, the following conclusions are obtained by analyzing the dynamic characteristics of inertia symmetric rotor and inertia asymmetric rotor with multiple loads after FBO occurs:

- (1) The load characteristics of the blade are described in detail after FBO occurs, and the rotor dynamic model of inertia symmetric rotor and inertia asymmetric rotor with multiple load excitation is established.
- (2) After the blade loss, the vibration response of aero-engine rotor system is the largest when it decelerates passing the critical speed, which is also the most dangerous point; With the action of multiple load excitation, the rotor system will appear backward whirl frequency for the excitation of rub-impact.
- (3) With the action of multiple load excitation, the vibration response of the inertia asymmetric rotor is greater than that of the inertia symmetric rotor. and the peak reaction forces of No.1, No. 2 and No. 3 supports increase by 39.79%, 28.81% and 37.85% respectively.
- (4) Compared with the inertia symmetric rotor system, the inertia asymmetric rotor system has more serious rub-impact between rotor and stator; The inertia symmetric rotor mainly rubs in the form of contact non-separation full-cycle rubs, while the inertia asymmetric rotor mainly rubs in the form of contact separation local rub with multiple load excitation; The inertia asymmetric rotor system shows backward whirl characteristics with the action of multiple loads.

- (5) A safety design idea of the support structure is proposed, and the vibration response of the rotor is effectively reduced by reducing the No. 1 support stiffness and increasing the No. 1 support damping.

Acknowledgements. The authors would like to acknowledge the financial support from the National Science and Technology Major Project of the Ministry of Science and Technology of China (Grant Nos. J2019-VIII-0008-0169, Y2019-VIII-0011-0172 and 2017-I-0008-0009).

References

1. Yu, P., et al.: Dynamic modeling and vibration characteristics analysis of the aero-engine dual-rotor system with fan blade out. *Mech. Syst. Signal Process.* **106**, 158–175 (2018)
2. Genta, G.: *Dynamics-of-Rotating Systems*. Springer, Heidelberg (2005). <https://doi.org/10.1007/0-387-28687-X>
3. Ren, X.M., Gu, J.L.: Response of suddenly applied unbalance for aeroengine -bearing system. *J. Vibr. Eng.* **4**(3), 75–82 (1991)
4. Gu, J., Ren, X.M.: A study on solution of suddenly applied unbalance response of a rotor-support system. *Chinese J. Appl. Mech.* **8**(4), 56–62 (1991)
5. Liu, D., Hong, J., Su, Z., et al.: Dynamic characteristics of inertia asymmetry rotor and safety design. *J. Propul. Technol.* **43**(4), 200269 (2022)
6. Ikeda, T., Murakami, S.: Dynamic response and stability of a rotating asymmetric shaft mounted on a flexible base. *Nonlinear Dyn.* **20**(1), 1–19 (1999). <https://doi.org/10.1023/A:1008302203981>
7. Muszynska, A.: *Rotordynamics*. Taylor & Francis, New York (2005)
8. Beatty, R.F.: Differentiating rotor response due to radial rubbing. *J. Vibr. Acoust.* **107**(2), 151–160 (1985)
9. Zhang, S.Q., Lu, Q.S., Wang, Q.: Analysis of rub-impact events for a rotor eccentric from the case. *J. Vibr. Eng.* **11**(4), 492–496 (1998)
10. Liu, D., Li, C., Yang, H., et al.: Analysis of backward whirl for rubbing rotor caused by excitation of sudden unbalance. *J. Aerosp. Power* **36**(7), 1509–1519 (2021)
11. Sinha, S.K.: Rotordynamic analysis of asymmetric turbofan rotor due to fan blade-loss event with contact-impact rub loads. *J. Sound Vib.* **332**(9) (2013)
12. Li, C., Liu, D., et al.: Dynamic characteristics of flexible rotor and safety design of support structure with fan blade-off. *J. Aerosp. Power* **35**(11), 2263–2274 (2020)
13. Hong, J., Xu, M.-L., et al.: Structure safety design strategy of rotor-support system due to fan blade loss. *J. Aerosp. Power* **31**(11), 2273–2730 (2016)
14. Thiery, F., Gustavsson, R., Aidanpää, J.O.: Dynamics of a misaligned Kaplan turbine with blade-to-stator contacts. *Int. J. Mech. Sci.* **99**, 251–261 (2015)